

# How to pin down the CP quantum numbers of a Higgs boson in its tau decays at the LHC

S. Berge<sup>\*1</sup>, W. Bernreuther<sup>†2</sup>, B. Niepelt<sup>\*</sup> and H. Spiesberger<sup>\*3</sup>

<sup>\*</sup> Institut für Physik (WA THEP), Johannes Gutenberg-Universität, 55099 Mainz, Germany

<sup>†</sup> Institut für Theoretische Physik, RWTH Aachen University, 52056 Aachen, Germany

## Abstract

We investigate how the  $CP$  quantum numbers of a neutral Higgs boson or spin-zero resonance  $\Phi$ , produced at the CERN Large Hadron Collider, can be determined in its  $\tau$ -pair decay mode  $\Phi \rightarrow \tau^- \tau^+$ . We use a method [1] based on the distributions of two angles and apply it to the major 1-prong  $\tau$  decays. We show for the resulting dilepton, lepton-pion, and two-pion final states that appropriate selection cuts significantly enhance the discriminating power of these observables. From our analysis we conclude that, provided a Higgs boson will be found at the LHC, it appears feasible to collect the event numbers needed to discriminate between a  $CP$ -even and  $CP$ -odd Higgs boson and/or between Higgs boson(s) with  $CP$ -conserving and  $CP$ -violating couplings after several years of high-luminosity runs.

PACS numbers: 11.30.Er, 12.60.Fr, 14.80.Bn, 14.80.Cp

Keywords: hadron collider physics, Higgs bosons, tau leptons, parity, CP violation

---

<sup>1</sup>berge@uni-mainz.de

<sup>2</sup>breuther@physik.rwth-aachen.de

<sup>3</sup>spiesber@uni-mainz.de

## I. INTRODUCTION

If the Large Hadron Collider (LHC) at CERN will reach its major physics goal of discovering a spin-zero resonance, the next step will be to clarify the question whether this is the standard model (SM) Higgs-boson or some nonstandard resonance, as predicted by many of the presently discussed new physics scenarios. (For reviews, see [2–6].) Part of the answer to this question will be given by measuring the  $CP$  quantum numbers of such a particle. There have been a number of proposals and investigations on how to determine these quantum numbers for Higgs-like resonances  $\Phi$ , for several production and decay processes at hadron colliders, including Refs. [1, 7–19]. (For an overview, see [20].) It is the purpose of this article to study a method [1] with which one can pin down whether such a state  $\Phi$  is  $CP$ -even,  $CP$ -odd, or a  $CP$ -mixture, namely in its decays into  $\tau$ -lepton pairs with subsequent 1-prong decays.

Our investigations below are applicable to neutral spin-zero resonances  $h_j$ , for instance to the Higgs-boson(s) of the standard model and extensions thereof, with flavor-diagonal couplings to quarks and leptons as described by the Yukawa Lagrangian

$$\mathcal{L}_Y = -(\sqrt{2}G_F)^{1/2} \sum_{j,f} m_f (a_{jf} \bar{f} f + b_{jf} \bar{f} i \gamma_5 f) h_j. \quad (1)$$

Here  $m_f$  is the mass of the fermion  $f$  and we normalize the coupling constants to the Fermi constant  $G_F$ . A specific model is selected by prescribing the reduced scalar and pseudoscalar Yukawa coupling constants  $a_{jf}$  and  $b_{jf}$ . In the standard model (SM) with its sole Higgs-boson,  $j = 1$  and  $a_{jf} = 1$ ,  $b_{jf} = 0$ . Many SM extensions predict more than one neutral spin-zero state and the couplings (1) can have more general values. Two-Higgs doublet models, for instance, the nonsupersymmetric type-II models and the minimal supersymmetric SM extension (MSSM, see, e.g., [2–4, 20]) contain three physical neutral Higgs fields  $h_j$ . If the Higgs sector of these models is  $CP$ -conserving, or if Higgs-sector  $CP$  violation (CPV) is negligibly small, then the fields  $h_j$  describe two scalar states, usually denoted by  $h$  and  $H$ , with  $b_{jf} = 0$ ,  $a_{jf} \neq 0$ , and a pseudoscalar, denoted by  $A$ , with  $a_{jf} = 0$ ,  $b_{jf} \neq 0$ . In the case of Higgs-sector CPV, the mass eigenstates  $h_j$  are  $CP$  mixtures and have nonzero couplings  $a_{jf} \neq 0$  and  $b_{jf} \neq 0$  to scalar and pseudoscalar fermion currents. This would lead to  $CP$ -violating effects in the decays  $h_j \rightarrow f \bar{f}$  already at Born level [9].

In the following, we use the generic symbol  $\Phi$  for any of the neutral Higgs-bosons  $h_j$  of the models mentioned above or, in more general terms, for a neutral spin-zero resonance. At the LHC, a  $\Phi$  resonance can be produced, for instance, in the gluon and gauge boson fusion processes  $gg \rightarrow \Phi$  and  $q_i q_j \rightarrow \Phi q'_i q'_j$ , as well as in association with a heavy quark pair,  $t \bar{t} \Phi$  or  $b \bar{b} \Phi$ . Recent studies on Higgs-boson production and decay into  $\tau$  leptons within the SM and the MSSM include [21, 22]. Our method for determining the  $CP$  parity of  $\Phi$  can be applied to these and to any other LHC  $\Phi$ -production processes.

The spin of a resonance  $\Phi$  can be inferred from the polar angle distribution of the  $\Phi$ -decay

products. In its decays to  $\tau$  leptons,  $\Phi \rightarrow \tau^- \tau^+$ , which is a promising LHC search channel for a number of nonstandard Higgs scenarios (see, e.g. [3, 6] and the recent LHC searches [23, 24])  $\tau$ -spin correlations induce specific angular distributions and correlations between the directions of flight of the charged  $\tau$ -decay products, in particular an opening angle distribution and a  $CP$ -odd triple correlation and associated asymmetries [9, 14]. Once a resonance  $\Phi$  is discovered, these observables can be used to determine whether it is a scalar, a pseudoscalar, or a  $CP$  mixture.

The discriminating power of these observables can be exploited fully if the  $\tau^\pm$  rest frames, i.e., the  $\tau$  energies and three-momenta can be reconstructed. At the LHC this is possible for  $\tau$  decays into three charged-pions. With these decay modes the  $CP$  properties of a Higgs-boson resonance can be pinned down efficiently [18]. For  $\tau$  decays into one charged particle the determination of the  $\tau^\pm$  rest frames is, in general, not possible at the LHC. For the 1-prong decays  $\tau^\pm \rightarrow a^\pm$  the  $a^+ a^-$  zero-momentum frame can, however, be reconstructed. In [1] two observables, to be determined in this frame, were proposed and it was shown, for the direct decays  $\tau^+ \tau^- \rightarrow \pi^+ \pi^- \bar{\nu}_\tau \nu_\tau$ , that the joint measurement of these two observables determines the  $CP$  nature of  $\Phi$ . It will even be possible to distinguish (nearly) mass-degenerate scalar and pseudoscalar Higgs-bosons with  $CP$ -invariant couplings from one or several  $CP$  mixtures.

In this paper we analyze the  $\tau$ -pair decay mode of  $\Phi$  for all major 1-prong  $\tau$ -decays  $\tau^\pm \rightarrow a^\pm$  and investigate how this significantly larger sample can be used for pinning down the  $CP$  quantum numbers of  $\Phi$  in an efficient way. As the respective observables originate from  $\tau$ -spin correlations, the  $\tau$ -spin analyzing power of the charged particle  $a$  is crucial for this determination. The  $\tau$ -spin analyzing power of the charged lepton in the leptonic  $\tau$  decays and of the charged-pion in the 1-prong hadronic decays  $\tau^\pm \rightarrow \rho^\pm, a_1^\pm \rightarrow \pi^\pm$  is rather poor when integrated over the energy spectrum of the respective charged prong. Thus, the crucial question in this context is whether experimentally realizable cuts can be found such that, on the one hand, the  $\tau$ -spin analyzing power of the charged prongs is significantly enhanced and, on the other hand, the data sample is not severely reduced by these cuts. We have studied this question in detail and found a positive answer.

The paper is organized as follows. In the next section we briefly describe the matrix elements on which our Monte Carlo event simulation is based, and we recapitulate the two observables with which the  $CP$  nature of a Higgs-boson can be unraveled. In Sec. III we analyze in detail the distribution that discriminates between a scalar and pseudoscalar Higgs-boson, both for dilepton, lepton-pion, and two-pion final states, for several cuts. We demonstrate for a set of “realistic”, i.e., experimentally realizable cuts that the objectives formulated above can actually be met. This is then also shown for the distribution that discriminates between  $\Phi$  bosons with  $CP$ -violating and -conserving couplings. We conclude in Sec. IV.

## II. DIFFERENTIAL CROSS SECTION AND OBSERVABLES

We consider the production of a spin-zero resonance  $\Phi$  – in the following collectively called a Higgs-boson – at the LHC, and its decay to a pair of  $\tau^\pm$  leptons:

$$pp \rightarrow \Phi + X \rightarrow \tau^- \tau^+ + X. \quad (2)$$

The decays of  $\tau^\pm$  are dominated by 1-prong modes with an electron, muon, or charged-pion in the final state. We take into account the following modes, which comprise the majority of the 1-prong  $\tau$  decays:

$$\begin{aligned} \tau &\rightarrow l + \nu_l + \nu_\tau, \\ \tau &\rightarrow a_1 + \nu_\tau \rightarrow \pi + 2\pi^0 + \nu_\tau, \\ \tau &\rightarrow \rho + \nu_\tau \rightarrow \pi + \pi^0 + \nu_\tau, \\ \tau &\rightarrow \pi + \nu_\tau. \end{aligned} \quad (3)$$

In the following  $a^\mp = l^\mp, \pi^\mp$  refer to the charged prongs in the decays (3).

The hadronic differential cross section  $d\sigma$  for the combined production and decay processes (2), (3) can be written as a convolution of parton distribution functions and the partonic differential cross section  $d\hat{\sigma}$  for  $p_1 p_2 \rightarrow \Phi \rightarrow \tau^+ \tau^- \rightarrow a^+ a'^- + X$  (where  $p_1$  and  $p_2$  are gluons or (anti)quarks):

$$\begin{aligned} d\hat{\sigma} &= \frac{\sqrt{2}G_F m_\tau^2 \beta_\tau}{64\pi^2 s} d\Omega_\tau \overline{\sum} |M(p_1 p_2 \rightarrow \Phi + X)|^2 |D^{-1}(\Phi)|^2 \text{Br}_{\tau^- \rightarrow a'^-} \text{Br}_{\tau^+ \rightarrow a^+} \quad (4) \\ &\times \frac{dE_{a'^-} d\Omega_{a'^-}}{2\pi} \frac{dE_{a^+} d\Omega_{a^+}}{2\pi} n(E_{a^+}) n(E_{a'^-}) \\ &\times \left( A + b(E_{a'^-}) \mathbf{B}^+ \cdot \hat{\mathbf{q}}^- - b(E_{a^+}) \mathbf{B}^- \cdot \hat{\mathbf{q}}^+ - b(E_{a'^-}) b(E_{a^+}) \sum_{i,j=1}^3 C_{ij} \hat{q}_i^- \hat{q}_j^+ \right). \end{aligned}$$

Here,  $\sqrt{s}$  is the partonic center-of-mass energy,  $\beta_\tau = \sqrt{1 - 4m_\tau^2/p_\Phi^2}$ ,

$$\overline{\sum} |M(p_1 p_2 \rightarrow \Phi + X)|^2 \quad \text{and} \quad D^{-1}(\Phi) = (p_\Phi^2 - m_\Phi^2 + im_\Phi \Gamma_\Phi^{\text{tot}})^{-1} \quad (5)$$

is the spin and color averaged squared production matrix element and the Higgs-boson propagator, respectively, with  $m_\Phi$ ,  $p_\Phi^\mu$  and  $\Gamma_\Phi^{\text{tot}}$  denoting the Higgs-boson mass, its 4-momentum and its total width<sup>4</sup>. The squared matrix element  $|T|^2$  of the decay  $\Phi \rightarrow \tau^+ \tau^- X$ , integrated over  $X$ , is of the form

$$|T|^2 = \sqrt{2}G_F m_\tau^2 (A + B_i^+ \hat{s}_i^+ + B_i^- \hat{s}_i^- + C_{ij} \hat{s}_i^+ \hat{s}_j^-), \quad (6)$$

<sup>4</sup> Equation (4) holds as long as nonfactorizable radiative corrections that connect the production and decay stage of  $\Phi$  are neglected.

$\Phi$	$A$	$c_1$	$c_2$	$c_3$
scalar	$a_\tau^2 p_\Phi^2 \beta_\tau^2 / 2$	$a_\tau^2 p_\Phi^2 \beta_\tau^2 / 2$	$-a_\tau^2 p_\Phi^2 \beta_\tau^2$	0
pseudoscalar	$b_\tau^2 p_\Phi^2 / 2$	$-b_\tau^2 p_\Phi^2 / 2$	0	0
$CP$ mixture	$(a_\tau^2 \beta_\tau^2 + b_\tau^2) p_\Phi^2 / 2$	$(a_\tau^2 \beta_\tau^2 - b_\tau^2) p_\Phi^2 / 2$	$-a_\tau^2 p_\Phi^2 \beta_\tau^2$	$-a_\tau b_\tau p_\Phi^2 \beta_\tau$

Table I: Tree-level coefficients of the squared decay matrix element (6), (7) for  $\Phi = H, A$  (scalar, pseudoscalar) and for a  $CP$  mixture.

where  $\hat{\mathbf{s}}^\pm$  are the normalized  $\tau^\pm$  spin vectors in the respective  $\tau^\pm$  rest frames. The dynamics of the decay is encoded in the coefficients  $A, B_i^\pm$  and  $C_{ij}$ . Rotational invariance implies that

$$\mathbf{B}^\pm = B^\pm \hat{\mathbf{k}}^-, \quad C_{ij} = c_1 \delta_{ij} + c_2 \hat{k}_i^- \hat{k}_j^- + c_3 \epsilon_{ijl} \hat{k}_l^-, \quad (7)$$

where  $\mathbf{k}^-$  ( $\hat{\mathbf{k}}^-$ ) is the (normalized)  $\tau^-$  momentum in the  $\tau^+ \tau^-$  zero-momentum frame (ZMF). At tree level,  $B^\pm = 0$ . (A nonzero absorptive part of the amplitude, induced for instance by the photonic corrections to  $\Phi \rightarrow \tau\tau$  renders these coefficients nonzero, but the effect is very small [14].) The tree-level coefficients  $A$  and  $c_{1,2,3}$  induced by the general Yukawa couplings (1) are given in Table I (cf. also [14]) for a scalar ( $b_\tau = 0$ ) and a pseudoscalar ( $a_\tau = 0$ ) Higgs-boson,  $\Phi = H, A$ , and a  $CP$  mixture.

We use the narrow-width approximation for  $\tau^\pm$ . The branching ratios of the 1-prong  $\tau$  decays (3) are denoted by  $\text{Br}_{\tau^\pm \rightarrow a^\pm} = \Gamma_{\tau^\pm \rightarrow a^\pm} / \Gamma_\tau^{\text{tot}}$ . Moreover, the measure  $d\Omega_\tau = d\cos\theta_\tau d\varphi_\tau$  in (4) is the differential solid angle of the  $\tau^-$  in the Higgs rest frame, and  $d\Omega_{a^\pm} = d\cos\theta_{a^\pm} d\varphi_{a^\pm}$  and  $E_{a^\pm}$  is the differential solid angle and the energy of the charged prong  $a^\pm$  in the  $\tau^\pm$  rest frame. Furthermore, the functions  $n(E_{a^\mp})$  and  $b(E_{a^\mp})$  encode the decay spectrum of the respective 1-prong polarized  $\tau^\mp$  decay and are defined in the  $\tau^\mp$  rest frames by

$$\frac{d\Gamma(\tau^\mp(\hat{\mathbf{s}}^\mp) \rightarrow a^\mp(q^\mp) + X)}{\Gamma(\tau^\mp \rightarrow a^\mp + X) dE_{a^\mp} d\Omega_{a^\mp} / (4\pi)} = n(E_{a^\mp}) (1 \pm b(E_{a^\mp}) \hat{\mathbf{s}}^\mp \cdot \hat{\mathbf{q}}^\mp), \quad (8)$$

where  $\hat{\mathbf{q}}^\mp$  is the normalized momentum vector of the charged prong  $a^\mp$  in the respective frame. The function  $n(E_a)$  determines the decay rate of  $\tau \rightarrow a$  while  $b(E_a)$  encodes the  $\tau$ -spin analyzing power of the charged prong  $a = l, \pi$ . We call them spectral functions for short. They are given for the  $\tau$ -decay modes (3) in Appendix A. Using the spin-density matrix formalism, the combination of (6) and (8) yields, with (5), the formula (4).

The decay distribution (6) and the coefficients  $c_1, c_3$  of Table I imply that, at the level of the  $\tau^+ \tau^-$  intermediates states, the spin observables  $\hat{\mathbf{s}}^+ \cdot \hat{\mathbf{s}}^-$  and  $\hat{\mathbf{k}} \cdot (\hat{\mathbf{s}}^+ \times \hat{\mathbf{s}}^-)$  discriminate between a  $CP$ -even and  $CP$ -odd Higgs-boson, and between a Higgs-boson with  $CP$ -conserving and  $CP$ -violating couplings, respectively [9, 14]. At the level of the charged prongs  $a^+ a'^-$ , these correlations induce a nontrivial distribution of the opening angle  $\angle(\hat{\mathbf{q}}^+, \hat{\mathbf{q}}^-)$  and the  $CP$ -odd triple correlation  $\hat{\mathbf{k}} \cdot (\hat{\mathbf{q}}^+ \times \hat{\mathbf{q}}^-)$ , as can be read off from (4). The strength of these correlations depends on the product  $b(E_{a'^-})b(E_{a^+})$ , while  $n(E_{a'^-})n(E_{a^+})$  is jointly responsible for the

number of  $a^+a'^-$  events<sup>5</sup>.

A direct analysis of experimental data in terms of the kinematic variables used in the differential cross section Eq. (4) is not possible since the momenta of the  $\tau$  decay products are measured in the laboratory frame and the reconstruction of the  $\tau^\pm$  and  $\Phi$  rest frames is, in general, not possible. In Ref. [1] it was shown that one can, nevertheless, construct experimentally accessible observables with a high sensitivity to the  $CP$  quantum numbers of  $\Phi$ . The crucial point is to employ the zero-momentum frame of the  $a^+a'^-$  pair.

The distribution of the angle

$$\varphi^* = \arccos(\hat{\mathbf{n}}_\perp^{*+} \cdot \hat{\mathbf{n}}_\perp^{*-}) \quad (9)$$

discriminates between a  $J^{PC} = 0^{++}$  and  $0^{-+}$  state. Here  $\hat{\mathbf{n}}_\perp^{*\pm}$  are normalized impact parameter vectors defined in the zero-momentum frame of the  $a^+a'^-$  pair. These vectors can be reconstructed [1] from the impact parameter vectors  $\hat{\mathbf{n}}_\mp$  measured in the laboratory frame by boosting the 4-vectors  $n_\mp^\mu = (0, \hat{\mathbf{n}}_\mp)$  into the  $a'^-a^+$  ZMF and decomposing the spatial part of the resulting 4-vectors into their components parallel and perpendicular to the respective  $\pi^\mp$  or  $l^\mp$  momentum. We emphasize that  $\varphi^*$  defined in Eq. (9) is not the true angle between the  $\tau$  decay planes, but nevertheless, it carries enough information to discriminate between a  $CP$ -even and  $CP$ -odd Higgs-boson.

The role of the  $CP$ -odd and  $T$ -odd triple correlation mentioned above is taken over by the triple correlation  $\mathcal{O}_{CP}^* = \hat{\mathbf{p}}_-^* \cdot (\hat{\mathbf{n}}_\perp^{*+} \times \hat{\mathbf{n}}_\perp^{*-})$  between the impact parameter vectors just defined and the normalized  $a'^-$  momentum in the  $a'^-a^+$  ZMF, which is denoted by  $\hat{\mathbf{p}}_-^*$ . Equivalently, one can determine the distribution of the angle [1]

$$\psi_{CP}^* = \arccos(\hat{\mathbf{p}}_-^* \cdot (\hat{\mathbf{n}}_\perp^{*+} \times \hat{\mathbf{n}}_\perp^{*-})). \quad (10)$$

In an ideal experiment, where the energies of the  $\tau$  decay products  $a^\pm$  in the  $\tau^\pm$  rest frames would be known, one could determine the coefficients  $A$ ,  $B^\pm$ , and  $c_{1,2,3}$  by fitting the differential distribution (4) (using the SM input of the Appendix) to the data. However, due to missing energy in the final state, detector resolution effects and limited statistics, one has to average over energy bins. Moreover, for  $a^\mp \neq \pi^\mp$  the function  $b(E)$  is not positive (negative) definite, see below. Therefore, energy averaging can lead to a strong reduction of the sensitivity to the coefficients of  $b(E)$  in the differential cross section. A judicious choice of bins or cuts is therefore crucial to obtain maximal information on the  $CP$  properties of  $\Phi$ . We will discuss this in detail in the next section.

---

<sup>5</sup> The integral  $\int n(E_a)b(E_a)dE_a$  determines the overall  $\tau$ -spin analyzing-power of the particle  $a$ . It seems worth recalling that the physics of  $\tau$  decays, i.e., the  $V - A$  law, has been tested to a level of precision which is much higher than what is needed for our purposes. Therefore, when comparing predictions with future data, one can use the functions  $n(E_a)$  and  $b(E_a)$  of the Appendix as determined within the standard model.

### III. RESULTS

The observables (9) and (10) can be used for the 1-prong  $\tau$ -pair decay channels of any Higgs-boson production process at the LHC. We are interested here in the normalized distributions of these variables. If no detector cuts are applied, these distributions do not depend on the momentum of the Higgs-boson in the laboratory frame; i.e., these distributions are independent of the specific Higgs-boson production mode. Applying selection cuts, we have checked for some production modes (see below) that, for a given Higgs-boson mass  $m_\Phi \gtrsim 120$  GeV, the normalized distributions remain essentially process-independent (see also [1]).

For definiteness, we consider in the following the production of one spin-zero resonance  $\Phi$  at the LHC ( $\sqrt{S} = 14$  TeV) in a range of masses  $m_\Phi$  between 120 and 400 GeV. As we employ the general Yukawa couplings (1), our analysis below can be applied to a large class of models, including the standard model, type-II 2-Higgs doublet models, and the Higgs sector of the MSSM. Within a wide parameter range of type-II models,  $\Phi$  production is dominated by gluon-gluon fusion; for large values of the parameter  $\tan\beta = v_2/v_1$  (where  $v_{1,2}$  are the vacuum expectation values of the two Higgs doublet fields) the reaction  $b\bar{b} \rightarrow \Phi$  takes over. (For a recent overview of various Higgs-boson production processes and the state-of-the-art of the theoretical predictions, see, e.g., [25, 26]. Higgs-boson production and decay into  $\tau^- \tau^+$  was analyzed in the SM and MSSM in [21, 22], taking recent experimental constraints into account.)

For obtaining the results given below we have used the production processes  $b\bar{b} \rightarrow \Phi$  and  $gg \rightarrow \Phi$ . The reaction chains (2), (3) were computed using leading-order matrix elements only, but our conclusions will not change when higher-order QCD corrections are taken into account or other Higgs-boson production channels with large transverse momentum  $p_T^\Phi$  are considered. Our method can be applied to all production channels, because no reconstruction of the Higgs-boson momentum or the  $\tau$  momenta is needed for the determination of the distributions (9) and (10). Therefore, the method is applicable to Higgs-boson production with small or large transverse momentum, as long as the Higgs resonance can be identified in the  $\tau\tau$  events. (For a discussion of the background see the end of Sec. III D.)

If  $p_T^\Phi$  is small, the distributions can be measured as described below. If the  $\tau^-$ ,  $\tau^+$  decay into leptons or via a  $\rho$  or  $a_1$  meson, an approximate reconstruction of the Higgs-boson rest frame, as outlined in Sec. III C, will increase the discriminating power of the distributions, because appropriate cuts in this frame separate  $\tau$ -decay particles with large and small energies.

If  $p_T^\Phi$  is large, the reconstruction of the Higgs rest frame can be performed, see [27]. With similar cuts as used below, this leads to an even better discriminating power of the  $\varphi^*$  and  $\psi_{CP}^*$  distributions.

We have implemented Eq. (4) into a Monte Carlo simulation program which allows us to study the reconstruction of observables in a variety of reference frames and to impose selection cuts on momenta and energies.

In Sec. III A -III D we analyze, for the various 1-prong final states, the  $\varphi^*$  distributions for



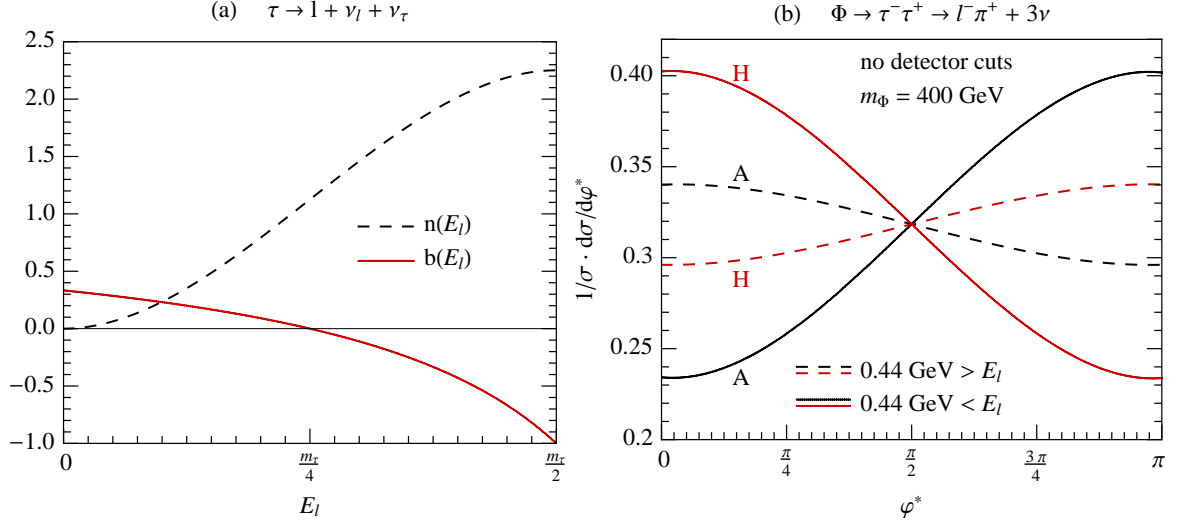


Figure 1: (a) The spectral functions  $n(E_l)$  and  $b(E_l)$ , Eq. (22), for the leptonic  $\tau$  decay. The function  $n(E_l)$  is given in units of  $\text{GeV}^{-1}$ . (b) The normalized  $\varphi^*$  distribution for  $l\pi$  final states without selection cuts in the laboratory frame for a Higgs mass of  $m_\Phi = 400$  GeV. A cut on the lepton energy in the  $\tau$  rest frame at  $m_\tau/4 \simeq 0.44$  GeV serves to show the effect of rejecting events where  $b(E_l)$  is positive and negative, respectively.

a scalar and pseudoscalar Higgs-boson, i.e., a spin-zero resonance  $\Phi$  with reduced Yukawa couplings  $a_\tau \neq 0, b_\tau = 0$  and  $a_\tau = 0, b_\tau \neq 0$ , respectively, to  $\tau$  leptons. For definiteness we choose  $a_\tau = 1$  and  $b_\tau = 1$ , respectively. The distribution of the  $CP$  angle  $\psi_{CP}^*$  is computed in Sec. III E for Higgs-bosons with  $CP$ -violating and  $CP$ -conserving couplings.

### A. Lepton-pion final state: $\tau\tau \rightarrow l\pi + 3\nu$

We start by discussing the case where the  $\tau^-$  from  $\Phi \rightarrow \tau^- \tau^+$  decays leptonically,  $\tau^- \rightarrow l^- + \bar{\nu}_l + \nu_\tau$ , and the  $\tau^+$  undergoes a direct decay into a pion,  $\tau^+ \rightarrow \pi^+ + \bar{\nu}_\tau$ . The purpose of this section is to study the shapes of the  $\varphi^*$  distributions for scalar and pseudoscalar Higgs-bosons when cuts are applied to the charged lepton; therefore, no cuts are applied at this point to the pion energy and momentum.

The charged lepton energy spectrum in the  $\tau \rightarrow l$  decay is determined by the functions  $n(E_l)$  and  $b(E_l)$  given in the Appendix, Eq. (22). These functions are shown in Fig. 1(a). One sees that the function  $b(E_l)$ , which determines the  $\tau$ -spin analyzing power of  $l$ , changes sign at  $E_l = m_\tau/4$ . Therefore also the slope of the resulting  $\varphi^*$  distribution for  $\pi l$  final states changes sign at this energy. The optimal way to separate a  $CP$ -even and  $CP$ -odd Higgs-boson would be to separately integrate over the energy ranges  $E_l > m_\tau/4$  and  $E_l < m_\tau/4$ . The resulting  $\varphi^*$  distributions for a scalar ( $H$ , red lines<sup>6</sup>) and pseudoscalar ( $A$ , black lines)

<sup>6</sup> Color in the electronic version.



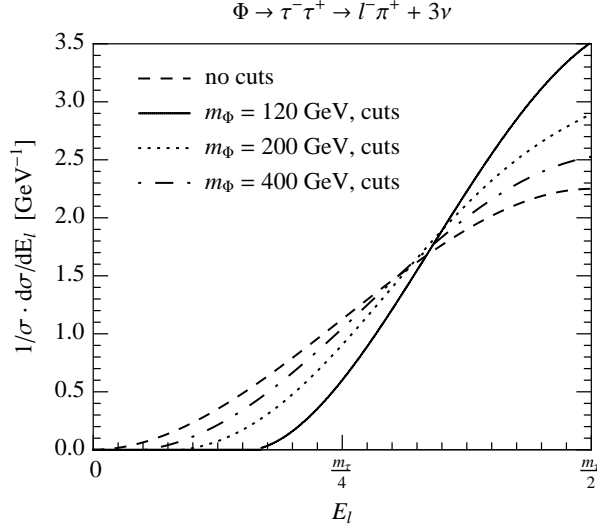


Figure 2: Normalized lepton energy distribution (in the  $\tau$  rest frame) for different Higgs-boson masses, with and without selection cuts (11).

Higgs-boson are shown in Fig. 1(b). For the energy range  $0 < E_l < m_\tau/4$ , the  $\varphi^*$  distribution has a positive (negative) slope for a scalar (pseudoscalar) Higgs-boson (dashed curves). For  $E_l > m_\tau/4$  the slopes change sign and the difference between a  $CP$ -even and a  $CP$ -odd boson becomes more pronounced (solid curves). However, at a LHC experiment, the separation of these two energy ranges is not possible because the  $\tau$  momenta can not be reconstructed and, therefore, the lepton energy  $E_l$  in the  $\tau$  rest frame can not be determined.

The difference between the  $\varphi^*$  distributions for a scalar and pseudoscalar Higgs-boson is, however, not completely washed out by integrating over the full lepton energy range, because both  $n(E_l)$  and  $b(E_l)$  have a significant energy dependence, see Fig. 1(a). The region  $0 < E_l < m_\tau/4$  contributes only about 19% to the decay rate  $\Gamma_{\tau \rightarrow l}$ ; in addition,  $b(E_l)$  is small in this energy range. Therefore, after integration over the full  $E_l$  range, the  $\varphi^*$  distribution is already quite close to the solid lines of Fig. 1(b). Moreover, one can suppress the contribution from the low-energy part of the spectrum by imposing a cut on the transverse momentum of the charged lepton in the laboratory frame. For the LHC experiments, suitable selection cuts on the transverse momentum and the pseudorapidity of the lepton in the  $pp$  frame are [23, 24]:

$$p_T^l = \sqrt{(p_x^l)^2 + (p_y^l)^2} \geq 20 \text{ GeV}, \quad |\eta_l| \leq 2.5. \quad (11)$$

The effect of these cuts on the normalized lepton energy distribution in the  $\tau^-$  rest frame is shown in Fig. 2. Rejecting events with small  $p_T^l$  preferentially removes events with small lepton energy in the  $\tau$  rest frame. The effect is more pronounced for light Higgs-boson masses where the  $\tau$  energy is smaller on average. For  $m_\Phi = 120$  GeV, only a small fraction of  $\pi l$  events with  $E_l < m_\tau/4$ , about 3.6%, survives the cuts (11). For  $m_\Phi = 200$  and 400 GeV the corresponding fractions are 9.4% and 14%, respectively. Events with  $E_l < m_\tau/4$  that

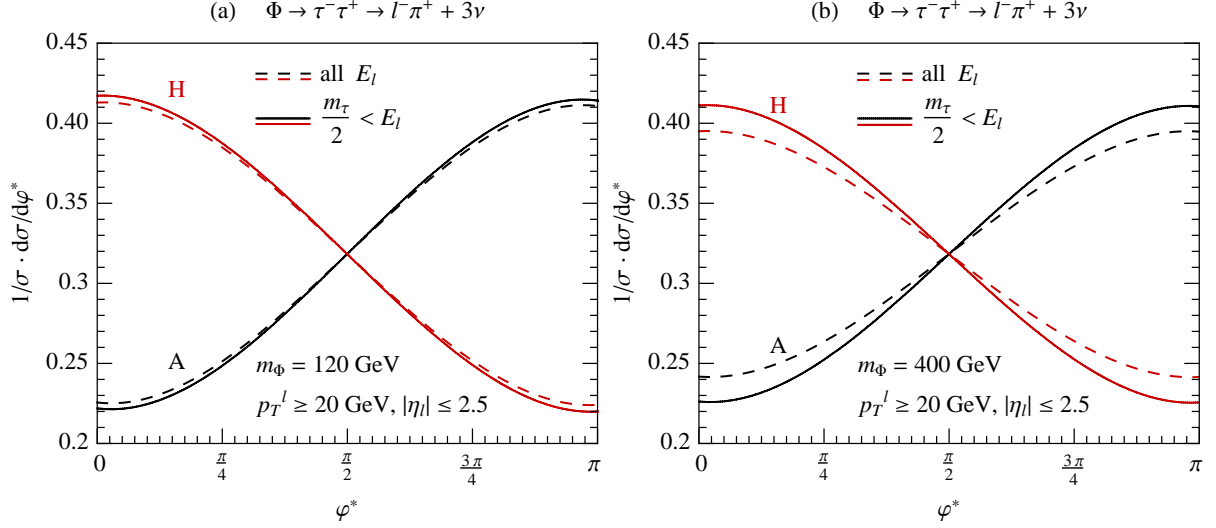


Figure 3: The normalized  $\varphi^*$  distributions for  $l\pi 3\nu$  final states. The solid (dashed) curves show the distribution with the cuts  $p_T^l > 20$  GeV and  $|\eta_l| < 2.5$  (without these cuts). (a)  $m_\Phi = 120$  GeV; (b)  $m_\Phi = 400$  GeV.

pass the above cuts have energies close to  $m_\tau/4$ , where the function  $b(E_l)$  is very small. The resulting  $\varphi^*$  distribution is almost unaffected by contributions with  $E_l < m_\tau/4$ , for Higgs masses up to 200 GeV. As an example, the  $\varphi^*$  distributions are displayed for  $m_\Phi = 120$  GeV in Fig. 3(a) and for  $m_\Phi = 400$  GeV in Fig. 3(b). From these results we conclude that only for very large Higgs-boson masses one can expect to improve the discrimination of scalar and pseudoscalar bosons by such a detector cut.

The experimentally relevant case, where in addition also selection cuts on the charged-pion are applied, will be discussed in Section III D.

### B. Hadronic final states: $\tau^- \tau^+ \rightarrow \{a_1^-, \rho^-, \pi^-\} \pi^+$

Next we analyze the case where the  $\tau^-$  decays to  $\pi^-$  either via a  $\rho$  meson,  $\tau^- \rightarrow \rho^- + \nu_\tau \rightarrow \pi^- + \pi^0 + \nu_\tau$ , an  $a_1$  meson,  $\tau^- \rightarrow a_1^- + \nu_\tau \rightarrow \pi^- + 2\pi^0 + \nu_\tau$ , or directly,  $\tau^- \rightarrow \pi^- + \nu_\tau$ , while  $\tau^+$  undergoes a direct 2-body decay,  $\tau^+ \rightarrow \pi^+ + \bar{\nu}_\tau$ . (The respective branching ratios are collected in Table V).

The spectral functions  $n(E_\pi)$  and  $b(E_\pi)$  for the  $\rho$  and  $a_1$  modes are given in the Appendix and shown in Fig. 4. The direct decay mode  $\tau^- \rightarrow \pi^- + \nu_\tau$  is characterized by a constant pion energy in the  $\tau$  rest frame and has maximal  $\tau$ -spin analyzing power  $b = 1$ .

As in the case of leptonic  $\tau$  decay the functions  $b_\rho(E_\pi)$  and  $b_{a_1}(E_\pi)$  change sign, at approximately 0.55 GeV. In contrast to the leptonic case, however, contributions from small pion energies are not suppressed by small differential rates, as evidenced by the functions  $n_\rho(E_\pi)$  and  $n_{a_1}(E_\pi)$ . At the LHC one will probably not be able to distinguish between the different 1-prong decay modes into a pion, at least not in an efficient way. Thus, one has to combine in

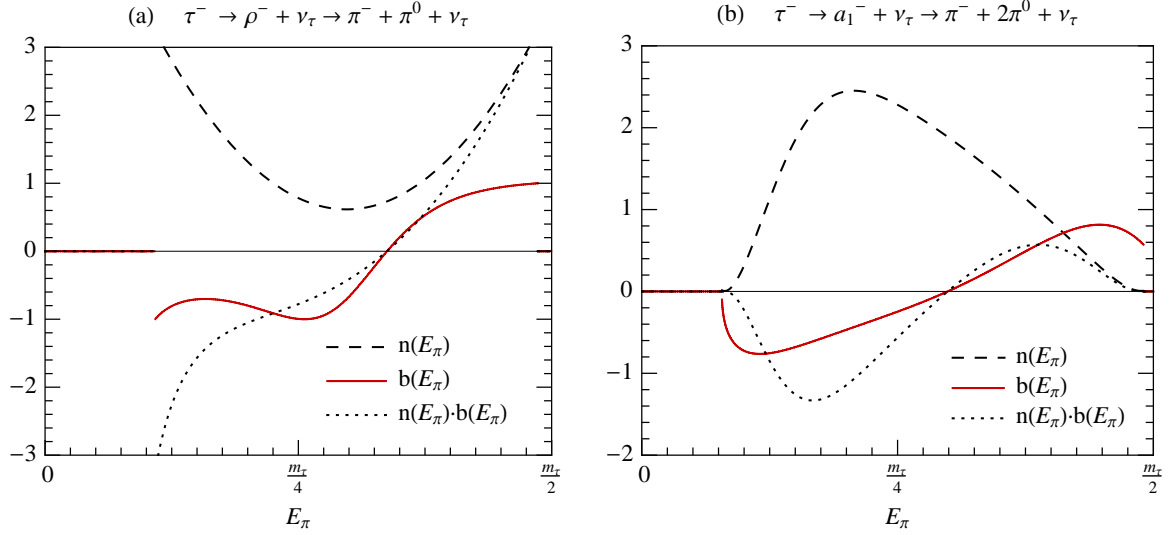


Figure 4: Charged-pion spectral functions  $n(E_\pi)$  and  $b(E_\pi)$  for hadronic  $\tau$  decays: (a)  $\tau^- \rightarrow \rho^- \nu_\tau \rightarrow \pi^- \pi^0 \nu_\tau$ ; (b)  $\tau^- \rightarrow a_1^- \nu_\tau \rightarrow \pi^- 2\pi^0 \nu_\tau$ . The functions  $n(E_\pi)$  and  $n(E_\pi)b(E_\pi)$  are given in units of  $\text{GeV}^{-1}$ .

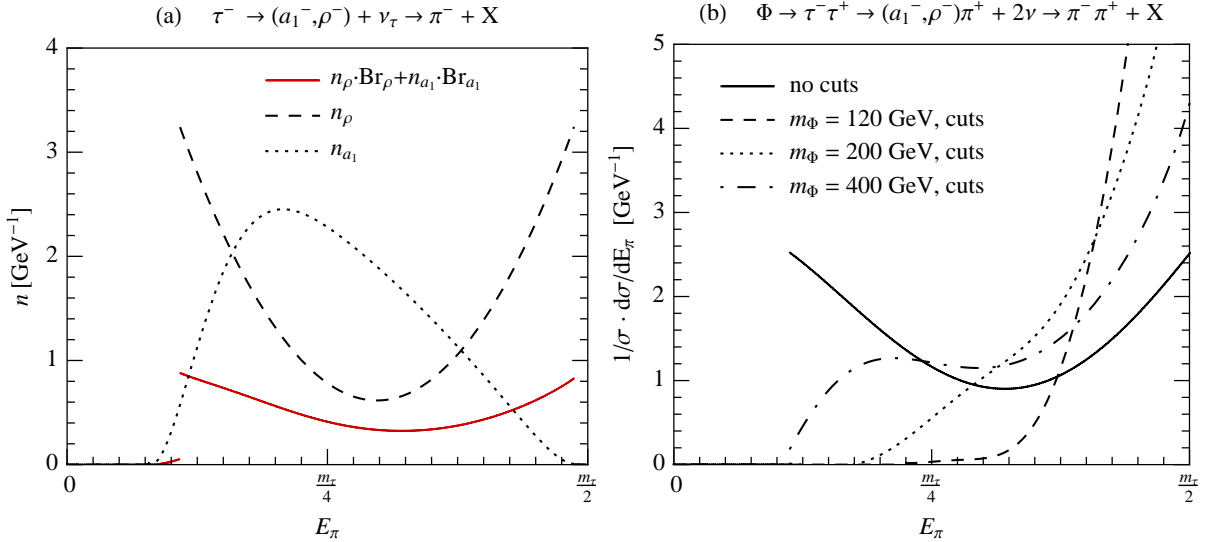


Figure 5: (a) Spectral function  $n(E_\pi)$  for the combined hadronic decay modes  $\tau \rightarrow a_1, \rho \rightarrow \pi$  (solid). (b) The distribution of the charged pion energy  $E_\pi$  for the combined  $a_1^-$  and  $\rho^-$  decays, for different Higgs-boson masses, with and without selection cuts.

the Monte Carlo modeling the different decay modes, weighted with their branching ratios. The combined functions  $n(E_\pi)$  for the decays  $\tau \rightarrow a_1$  and  $\tau \rightarrow \rho$  are shown in Fig. 5(a). The combined distribution is dominated by the  $\rho$  decay mode because of its larger branching ratio. The result (solid red curve) in Fig. 5(a) shows that contributions where  $E_\pi > 0.55 \text{ GeV}$  and  $E_\pi < 0.55 \text{ GeV}$ , i.e., where  $b(E_\pi)$  is positive and negative, respectively, are equally important. Without cuts, one would, as a consequence, not be able to distinguish between scalar and pseudoscalar Higgs-bosons by means of the  $\varphi^*$  distribution. Therefore we im-

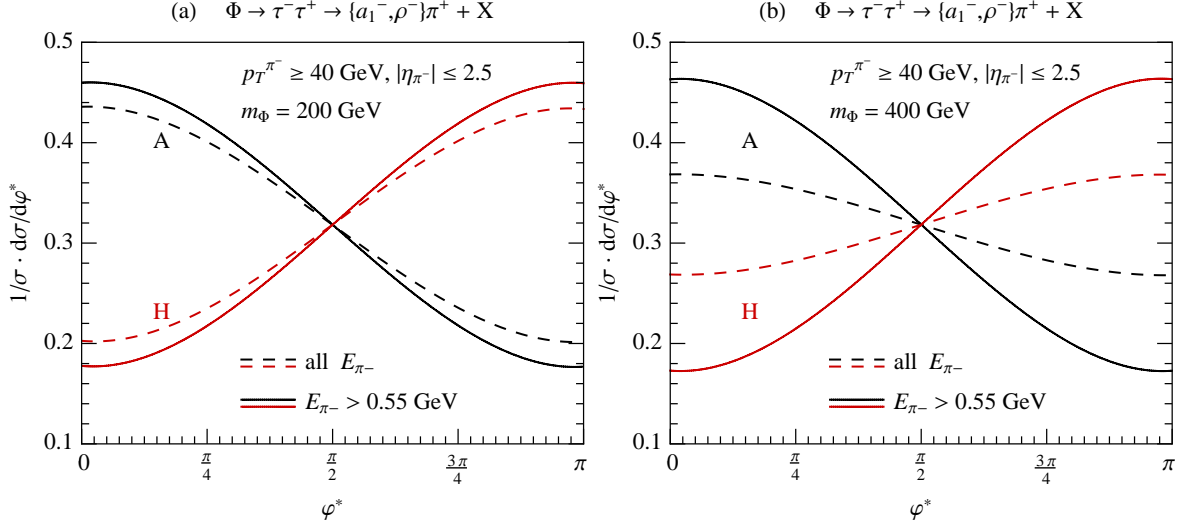


Figure 6: The normalized  $\varphi^*$  distributions for the combined decays  $\Phi \rightarrow \tau^- \tau^+ \rightarrow \{a_1^-, \rho^-\} \pi^+ \rightarrow \pi^- \pi^+$ . The  $p_T$  and  $\eta$  cuts (12) are imposed on  $\pi^-$  only (dashed curves). The solid curves show the distributions which result if instead of (12) an experimentally not feasible cut on the pion energy  $E_{\pi^-}$  in the  $\tau$  rest frame is applied. (a)  $m_\Phi = 200$  GeV; (b)  $m_\Phi = 400$  GeV.

pose the following selection cuts on the charged-pion in the  $pp$  laboratory frame, which are compatible<sup>7</sup> with the cuts used by the LHC experiments [23, 24]:

$$p_T^\pi \geq 40 \text{ GeV}, \quad |\eta_\pi| \leq 2.5. \quad (12)$$

At this point, the constraints (12) are imposed – for the purpose of analyzing the effect of these cuts – only on the  $\pi^-$  from  $\tau^-$  decays. These cuts will be applied to both  $\pi^-$  and  $\pi^+$  from  $\tau^-$  and  $\tau^+$  decays, respectively, in Section III D.

The impact of these cuts on the distribution  $\sigma^{-1} d\sigma/dE_\pi$  (where  $E_\pi$  is the energy of the  $\pi^-$  in the  $\tau^-$  rest frame) for the combined  $\tau^- \rightarrow a_1^-, \rho^- \rightarrow \pi^-$  decay modes is displayed in Fig. 5(b) for several Higgs-boson masses between 120 and 400 GeV. The solid curve shows the distribution without cuts; it does not depend on  $m_\Phi$ . The cuts (12) preferably reject events with small  $E_\pi$ . The effect of these cuts is strong for light Higgs-boson masses and still pronounced for  $m_\Phi \sim 200$  GeV.

As a consequence, the  $\varphi^*$  distributions are dominated by contributions with positive values of the  $\tau$ -spin analyzer functions  $b_\rho(E_\pi)$ ,  $b_{a_1}(E_\pi)$ , and the distributions clearly differ for  $\Phi = H$  and  $\Phi = A$ , see Fig. 6(a). For small Higgs-boson masses, the cuts (12) are almost as efficient as an experimentally not realizable cut on the pion energy in the  $\tau$  rest frame, as shown by the solid curves in Fig. 6(a). For heavy Higgs-bosons the discriminating power of the  $\varphi^*$  distributions decreases, see Fig. 6(b). This decrease can be avoided by an additional cut, as

<sup>7</sup> In fact, the searches [23, 24] used  $p_T^\pi > 20$  GeV; but our tighter  $p_T$  cut can, of course, always be applied in addition to the selected data sample.

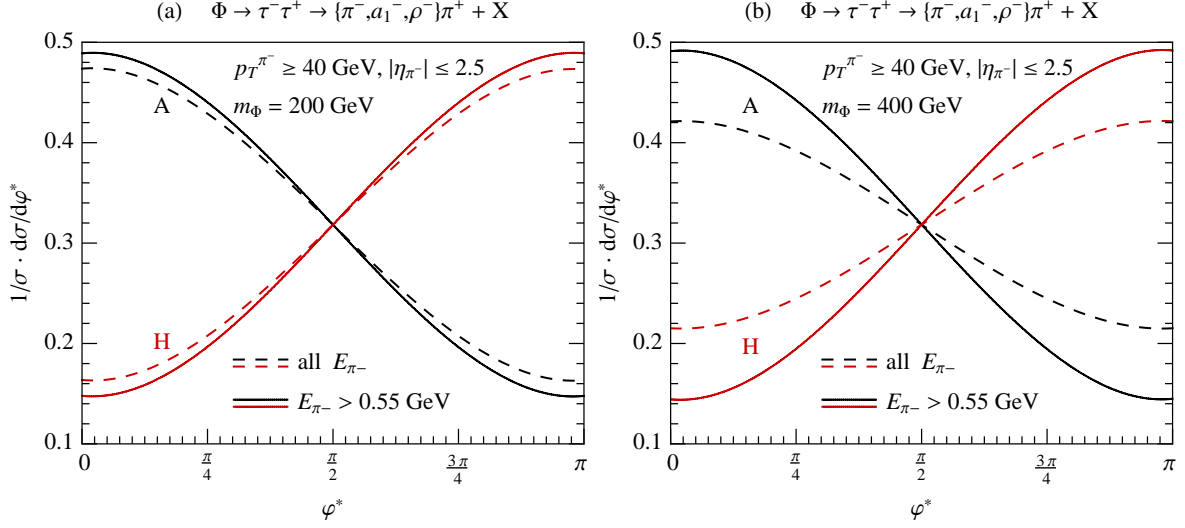


Figure 7: Same as Fig. 6, including the contribution from the direct decay  $\tau^- \rightarrow \pi^- \nu$ . (a)  $m_\Phi = 200$  GeV; (b)  $m_\Phi = 400$  GeV.

discussed in Sec. III C.

In fact, the situation is improved by taking into account the contribution from the direct decay  $\tau^- \rightarrow \pi^- + \nu_\tau$  which has maximal  $\tau$ -spin analyzing power. This decay channel is less strongly affected by the acceptance cuts (12) because the  $\pi^-$  energy in the  $\tau^-$  rest frame is  $E_{\pi^-} = m_\tau/2$ . This is shown by the ratio  $R$  of the contributions from the direct  $\pi^-$  and the  $\rho^- + a_1^-$  decays to the cross section  $pp \rightarrow \Phi \rightarrow \tau^- \tau^+$ , given for  $m_\Phi = 200$  GeV and  $m_\Phi = 400$  GeV in Table II. The numbers given in this table were computed at tree-level, but we expect them to not be strongly affected by radiative corrections to the  $\Phi$  production amplitude.

The  $\varphi^*$  distributions, with the direct  $\tau^- \rightarrow \pi^-$  contribution included, are shown in Fig. 7. Comparing with Fig. 6 we see that the discriminating power has indeed improved, both for small and large Higgs-boson masses. For  $m_H = 200$  GeV, the cuts (12) are in fact almost optimal, as one can see by comparing the dashed with the solid curves in Fig. 7.

The reconstruction of the  $\varphi^*$  distributions requires the determination of the (normalized) impact parameter vectors  $\mathbf{n}_-$  and  $\mathbf{n}_+$ . One may ask whether a cut on their length would improve the sensitivity of the data selected in this way. We have therefore performed a simulation, along the lines outlined in [1], where we require  $|\mathbf{n}_-| > 20 \mu m$  for the displacement of the secondary vertex of  $\tau^- \rightarrow \pi^-$ , assuming an exponential decay of the  $\tau$  with a mean life-time

ratio	$R_{no\ cuts}^{m_\Phi=200}$	$R_{p_T^{\pi^-}, \eta_{\pi^-} \text{ cuts}}^{m_\Phi=200}$	$R_{no\ cuts}^{m_\Phi=400}$	$R_{p_T^{\pi^-}, \eta_{\pi^-} \text{ cuts}}^{m_\Phi=400}$
$R = \sigma_{\tau^- \rightarrow \pi^-} / \sigma_{\tau^- \rightarrow \{a_1^-, \rho^-\} \rightarrow \pi^-}$	0.31	0.82	0.31	0.50

Table II: Ratio of different final-state contributions to the cross section for  $pp \rightarrow \Phi \rightarrow \tau^- \tau^+$  with and without detector cuts as described in the text.

of  $2.9 \cdot 10^{-13}s$ . However, it turns out that the  $\varphi^*$  distributions are only slightly affected – there is no gain in sensitivity. In addition, the cross section is reduced by almost a factor of 2. Therefore, we refrain from this requirement in the following.

### C. Reconstruction of approximate $\tau$ momenta

From the discussion in the previous section we conclude that a more refined event selection is desirable for large Higgs-boson masses of the order of 400 GeV. In particular, additional cuts that remove events with low-energy pions (referred to the respective  $\tau$  rest frame), where  $b(E_\pi)$  is negative, would help to improve the discrimination of  $CP$ -even and  $CP$ -odd resonances. Knowledge of the  $\tau^\mp$  4-momenta would allow us to Lorentz-boost the measured pion momenta to the respective  $\tau$  rest frame, where the application of a cut on  $E_\pi$  would be straightforward. An approximate reconstruction of the  $\tau$  momenta will be sufficient for this purpose, as long as it helps to enhance the difference of  $\varphi^*$  distributions for scalar and pseudoscalar Higgs-bosons. In the following we describe an approach where we combine the information contained in the measured pion momenta in the  $pp$  laboratory frame and the experimentally known value of the Higgs-boson mass.

We make the following approximations: i) In the laboratory frame, the  $\tau$  momenta  $\mathbf{k}^\pm$  and  $\pi$  momenta  $\mathbf{p}_\pm$  are collinear, i.e.,  $\mathbf{k}^\pm = \kappa_\pm \hat{\mathbf{p}}^\pm$ . ii) The measured missing transverse momentum  $\mathbf{P}_T^{miss}$  is assigned to the sum of the differences of the transverse momenta of  $\tau^\pm$  and the charged prong  $a^\pm$ , i.e.,  $\mathbf{P}_T^{miss} = \mathbf{k}_T^- - \mathbf{p}_T^- + \mathbf{k}_T^+ - \mathbf{p}_T^+$ . This is a very crude approximation for  $\tau \rightarrow \rho, a_1$ , but it serves the goal formulated above. One can then write down eight equations for the eight unknown components of the  $\tau^\pm$  4-momenta  $k^{\pm\mu}$ :

$$\begin{aligned} p_\Phi^\mu &= k^{+\mu} + k^{-\mu}, \\ m_\tau^2 &= (k^+)^2, \\ m_\tau^2 &= (k^-)^2, \\ \mathbf{P}_T^{miss} &= \mathbf{k}_T^- - \mathbf{p}_T^- + \mathbf{k}_T^+ - \mathbf{p}_T^+. \end{aligned}$$

These equations can be solved analytically. One obtains an approximate Higgs momentum  $p_\Phi^{\sim\mu}$  which can be used to boost the  $\pi$  momenta to the corresponding approximate Higgs-boson rest frame. We denote the resulting pion energies by  $E_{\pi^-}^\sim$ . The distribution of  $E_{\pi^-}^\sim$  is shown in Fig. 8(a). The upper solid (black) curve shows the distribution for the  $\rho + a_1$  decays without cuts, while the dotted curves result from imposing the cuts (12). The lower solid and dotted (red) curves display the corresponding distribution for the direct  $\tau^- \rightarrow \pi^- \nu$  decay. From this result and the analysis of the previous section we conclude that events with small pion energies in the  $\tau$  rest frames are correlated with events with small pion energies in the approximate Higgs-boson rest frame. This statement is supported by the distribution displayed in Fig. 8(b). This figure shows that, by imposing a cut on  $E_{\pi^-}^\sim$ , the distribution of  $E_{\pi^-}$  is shifted to larger values of the pion energy.

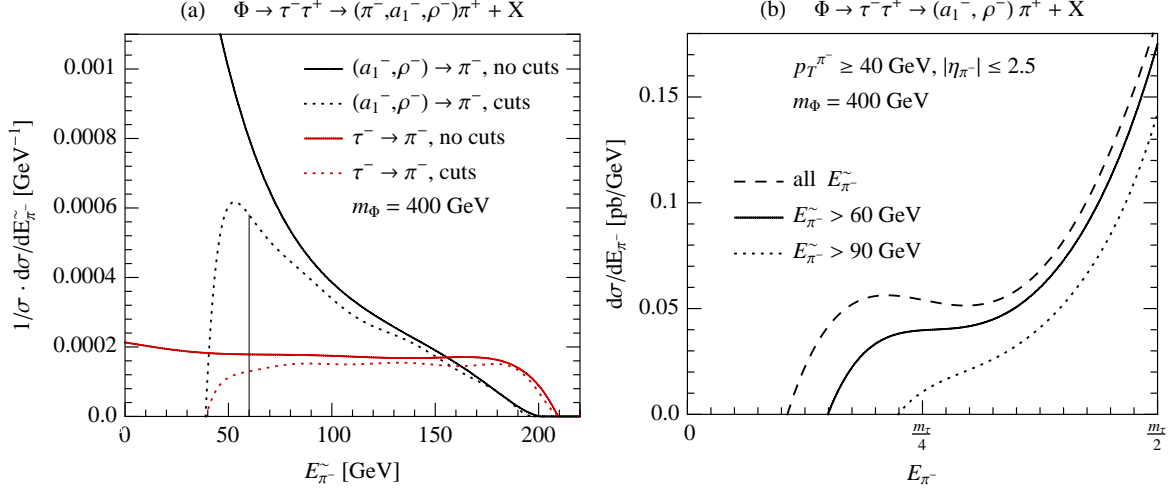


Figure 8: (a) Distribution of  $E_{\pi^-}$  in the approximate Higgs rest frame. The solid curves correspond to the distribution without cuts; the dotted curves are obtained when applying the cuts Eq. (12). The vertical line indicates the additional cut  $E_{\pi^-} = 60$  GeV. (b)  $E_{\pi^-}$  distribution for the combined decays  $\tau^- \rightarrow a_1^-, \rho^-$ , with cuts (12), with and without an additional cut on  $E_{\pi^-}$ .

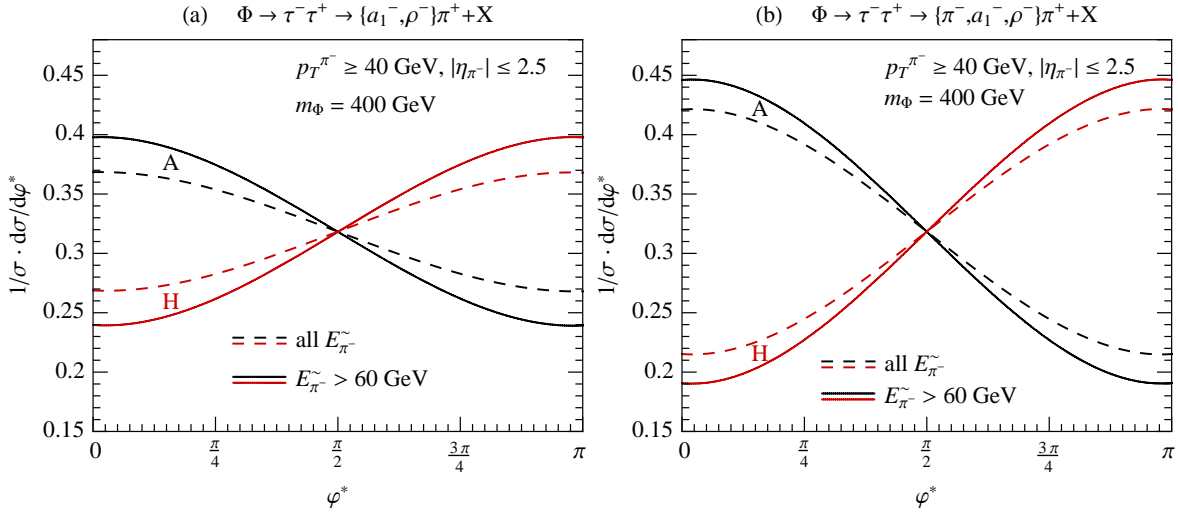


Figure 9: (a) The normalized  $\varphi^*$  distributions (without the direct  $\tau^- \rightarrow \pi^-$  decay) with and without a cut on the reconstructed pion energy  $E_{\pi^-}$ . The solid curves result from events with  $E_{\pi^-} > 60$  GeV. (b) Same as (a), but with the direct  $\tau^- \rightarrow \pi^-$  decay channel included.

Encouraged by these observations we calculate, for heavy Higgs-bosons, the normalized  $\varphi^*$  distributions by imposing the additional cut  $E_{\pi^-} > 60$  GeV. The results are shown in Fig. 9. For comparison, the dashed curves result from applying only the cuts (12). The additional cut of  $E_{\pi^-} > 60$  GeV clearly leads to an increase in sensitivity. Including the  $\tau \rightarrow \pi\nu$  decay leads to a further improvement, see Fig. 9(b). In fact, the additional cut affects the direct decay channel only marginally.

One should keep in mind that the additional cut on  $E_{\pi^-}$  will reduce the size of the event



samples for the measurement of the  $\varphi^*$  distributions. The sample based on  $\tau^- \rightarrow \rho^-, a_1^-$ , and  $\pi^-$  decays will be reduced by about 18%. An analysis including a full detector simulation is required in order to optimize the selection cuts (12) and the cut on  $E_{\pi}^{\sim}$ .

These conclusions will not be affected by analyzing different  $\Phi$  production processes or by taking into account higher-order QCD corrections. For example, let us consider the production of a Higgs-boson with very high  $p_T$  in the laboratory frame. Then the  $l^{\pm}$  and  $\pi^{\pm}$  from  $\tau^{\pm}$  decays can pass the transverse momentum cuts (11) and (12), even if the energies of the charged prongs in the respective  $\tau$  rest frames are small. As a result, contributions to the decay modes  $\tau \rightarrow l, a_1, \rho$  with  $b(E_{\pi, l}) > 0$  and  $b(E_{\pi, l}) < 0$  cancel and the discriminating power of the  $\varphi^*$  distribution is reduced. However, when applying an additional cut in the approximate Higgs rest frame as described above, the dangerous contributions will be rejected. This yields basically the same  $\varphi^*$  distributions as before. In addition, for Higgs events with large  $p_T$ , much better methods of reconstructing the  $\tau$  rest frame can be applied, for instance the collinear approximation [27] or the method described in [28]. High  $p_T$  particles/jets that are produced in association with a Higgs-boson can also be used to reconstruct an approximate Higgs rest frame.

#### D. Combined leptonic and hadronic 1-prong decays

In this section we present results for the  $\varphi^*$  distributions taking into account all 1-prong decays (3), i.e.,

$$pp \rightarrow \Phi \rightarrow \tau^- \tau^+ \rightarrow \begin{cases} l^- l'^+ + X, & l, l' = e, \mu, \\ l^- \pi^+ + X \text{ and } \pi^- l'^+ + X, \\ \pi^- \pi^+ + X. \end{cases} \quad (13)$$

We refer to the different channels in (13) by *dilepton*, *lepton-pion*, and *two-pion* final states. The cuts (11) and (12) are applied to the charged leptons and pions,  $l^{\mp}$  and  $\pi^{\mp}$ , respectively. For the dilepton final states the  $\varphi^*$  distributions are presented in Fig. 10(a) for two values of the Higgs-boson mass. The figure shows that the power of  $\varphi^*$  to discriminate between a scalar and pseudoscalar Higgs-boson is, in these decay channels, almost independent of the mass of  $\Phi$ . As discussed in Sec. III A, one would increase the sensitivity if one could reconstruct the  $\tau^{\mp}$  rest frames and select an event sample with an additional cut on the lepton energies in these frames. However, Fig. 10(b) shows that the enhancement would be rather modest.

In Fig. 11(a) and (b) the  $\varphi^*$  distributions are presented for the lepton-pion and two-pion final states, respectively, for two different values of the Higgs-boson mass. For these final states, the discriminating power of the  $\varphi^*$  distribution decreases with increasing Higgs-boson mass. We emphasize, however, that our evaluation is conservative in the sense that we applied only the acceptance cuts (11) and (12). As shown in Sec. III C, a further cut on the charged-pion energy  $E_{\pi}^{\sim}$  in the approximate Higgs-boson rest frame would significantly enhance the

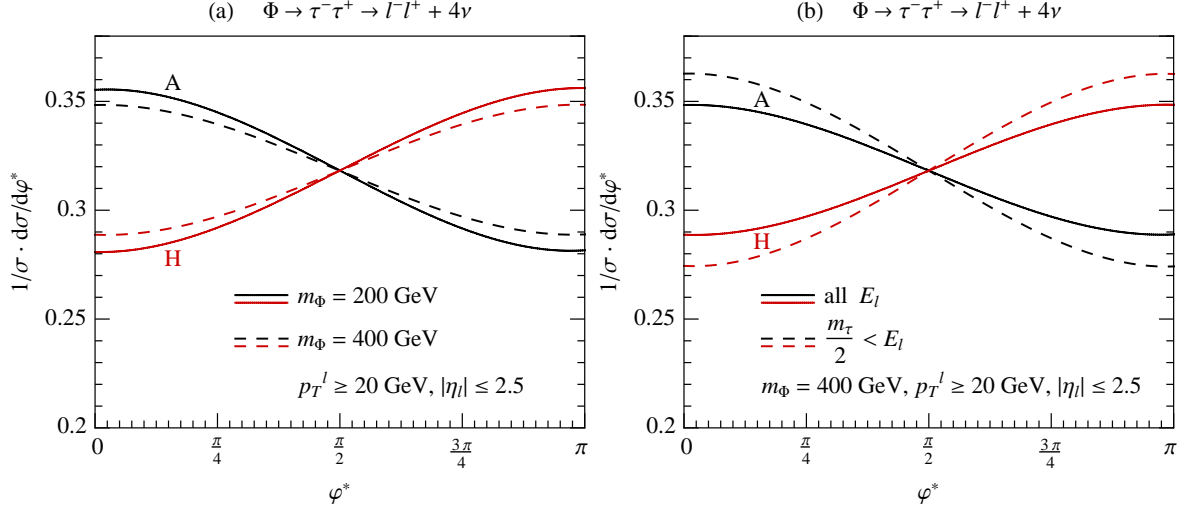


Figure 10: (a) The normalized  $\varphi^*$  distributions for the dilepton final states, for  $m_\Phi = 200$  GeV (solid curves) and  $m_\Phi = 400$  GeV (dashed curves). (b) The solid curves are identical to (a) for  $m_\Phi = 400$  GeV; the dashed curves result from applying an additional cut  $E_l > \frac{m_\tau}{2}$  on the charged lepton energies in the  $\tau^\mp$  rest frames.

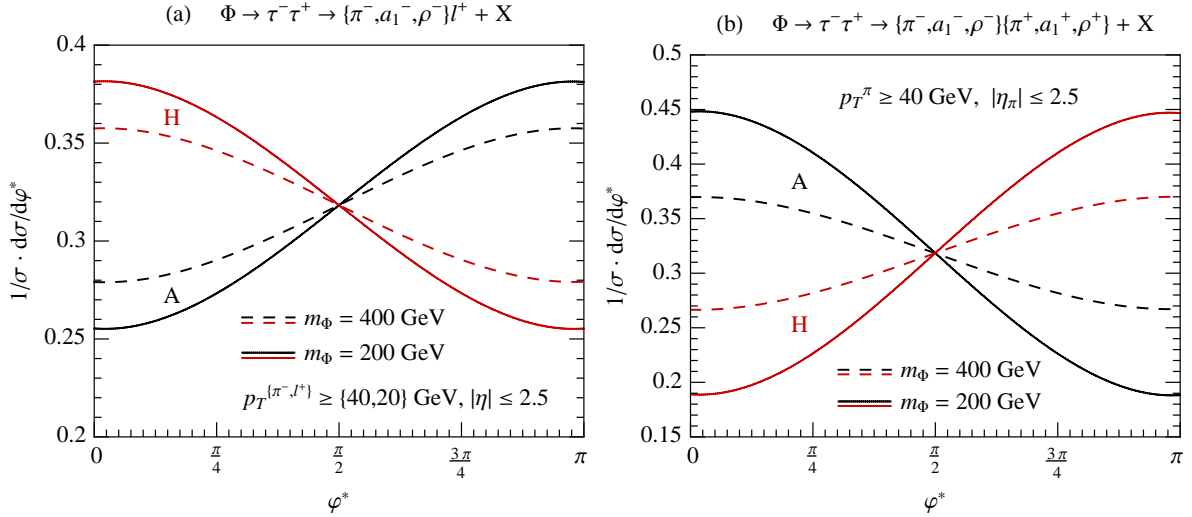


Figure 11: (a) The normalized  $\varphi^*$  distributions for the lepton-pion final states for  $m_\Phi = 200$  GeV (solid curves) and  $m_\Phi = 400$  GeV (dashed curves). (b) The  $\varphi^*$  distributions for the two-pion final states.

discriminating power of  $\varphi^*$  in the case of heavy Higgs-bosons or Higgs-bosons with large  $p_T$ .

Notice that the  $\varphi^*$  distributions for a scalar (pseudoscalar) Higgs-boson have opposite slopes for lepton-pion and two-pion final states. This is due to the fact that the signs of the leptonic and hadronic spin analyzer functions  $b(E_l)$  and  $b(E_\pi)$  differ, both in the low-energy and high-energy part of the spectrum. Therefore, a very good experimental discrimination of leptons and pions will be crucial for this measurement.

$m_\Phi$ [GeV]	dilepton	lepton-pion	two-pion
200	380	116	18
400	600	334	207

Table III: Event numbers needed to distinguish between a  $CP$ -even and  $CP$ -odd spin-zero state  $\Phi$  with 3 s.d. significance.

It should be noticed that i) a Higgs-boson with scalar and pseudoscalar  $\tau$ -Yukawa couplings of equal strength (i.e., an ideal  $CP$  mixture) or ii) (nearly) mass-degenerate scalar and pseudoscalar Higgs-bosons with equal production cross sections yield a  $\varphi^*$  distribution which is flat, both for dilepton, lepton-pion, and two-pion final states (cf. [1]). In order to unravel these possibilities, one has to measure the distribution of the angle  $\psi_{CP}^*$ , see below. The  $\varphi^*$  distributions of mass-degenerate scalars and pseudoscalars with different reaction cross sections and of a  $CP$  mixture with  $|a_\tau| \neq |b_\tau|$  have shapes which lie between the pure scalar and pseudoscalar cases and can also be disentangled with a joint measurement of the  $\psi_{CP}^*$  distribution.

Next, we make a crude estimate of how many events are needed in order to distinguish between a scalar and a pseudoscalar Higgs-boson in the different decay channels (13). We consider the asymmetry

$$A_{\varphi^*} = \frac{N(\varphi^* > \pi/2) - N(\varphi^* < \pi/2)}{N(\varphi^* > \pi/2) + N(\varphi^* < \pi/2)}. \quad (14)$$

The asymmetries can be computed for the different final states from the distributions Figs. 10(a), 11(a), and (b), for a scalar and a pseudoscalar Higgs-boson. Assuming that systematic effects can be neglected, we estimate from these asymmetries the event numbers needed to distinguish a scalar from a pseudoscalar Higgs-boson with 3 standard deviation (s.d.) significance. These numbers are given in Table III.

One may ask how vulnerable the  $\varphi^*$  distributions – and the  $\psi_{CP}^*$  distributions given in the next section – are with respect to uncertainties in the experimental determination of the  $\Phi$  production/decay vertex and of the energies and momenta of the charged prongs. This question was investigated in [1] for the direct pion decay modes  $\tau^- \tau^+ \rightarrow \pi^- \pi^+ \bar{\nu}_\tau \nu_\tau$  by a Monte Carlo simulation and it was found that these distributions retain their discriminating power when measurement errors are taken into account. One may assume that this result stays valid also for the larger class of 1-prong decay modes considered in this paper.

We close this section with a brief discussion of background reactions to the  $\Phi \rightarrow \tau^- \tau^+$  signal. These include QCD multijets,  $t\bar{t}$ , single top,  $W$  + jets,  $Z/\gamma^*$  + jets,  $WW$ ,  $WZ$ , and  $ZZ$  production. Among these,  $Z/\gamma^* \rightarrow \tau^- \tau^+$  (+ jets) constitutes an essentially irreducible background for a Higgs-boson with mass close to the  $Z$  mass. Most of this background can be distinguished from the signal by means of appropriate discriminating variables, in particular by reconstructing the  $\tau$ -pair invariant mass  $M_{\tau\tau}$  using a likelihood technique, with which a

mass resolution of  $\sim 21\%$  was achieved [23]. For Higgs-bosons with masses  $m_\Phi \gtrsim 200$  GeV, the  $Z^* \rightarrow \tau^- \tau^+$  background can be suppressed by appropriate cuts on  $M_{\tau\tau}$ , which works also for purely hadronic  $\tau^- \tau^+$  decays [29].

If a Higgs-boson will be found with a mass not too far away from the  $Z$  mass one may, in the long run of the LHC, resort to the production of  $\Phi$  by vector boson fusion, in order to study the above distributions. In vector boson fusion,  $\Phi$  is produced in the central region, which provides a good veto against QCD background. More importantly, one has an additional signature from two well-separated forward jets, which gives a veto against  $Z^* \rightarrow \tau^- \tau^+$ . Yet, in the SM and for large portions of the parameter spaces of models with an extended Higgs sector,  $gg \rightarrow \Phi$  (and  $b\bar{b} \rightarrow \Phi$  for large  $\tan\beta$ ) is by far the dominant  $\Phi$  production process. The modulus of the pseudorapidity,  $|\eta|$ , of a light Higgs-boson produced in these reactions is large, while its transverse momentum, generated by QCD radiation, is small on average. The  $\tau\tau$  pair from  $\Phi \rightarrow \tau^- \tau^+$  is balanced in its total transverse momentum and its sum of the azimuthal angles. This provides a good discrimination against the QCD background, but not against  $Z \rightarrow \tau^- \tau^+$ . At this point one may exploit spin effects. The chiral-invariant  $Z\tau\tau$  and  $\gamma\tau\tau$  couplings lead to characteristic  $\tau\tau$  spin correlations (see, for instance, [30–33]) which differ from those that result from the decay of a spin-zero resonance whose fermion couplings are chirality-flipping. For instance, for the decays  $\tau^- \tau^+ \rightarrow \pi^- \pi^+ \nu\bar{\nu}$ , this has the following consequence. If the  $\pi^- \pi^+$  result from  $Z$  boson decay, the number of  $\pi^- \pi^+$  events with  $E_{\pi^-}$  and  $E_{\pi^+}$  both large or both small (in the  $\tau^- \tau^+$  ZMF) is much larger than the number of events with  $E_{\pi^-}$  large (small) and  $E_{\pi^+}$  small (large); while for  $\Phi \rightarrow \tau^- \tau^+$  just the opposite is the case. These  $\pi\pi$  energy distributions may be used to discriminate the signal from the irreducible background in the case of a light  $\Phi$ . In addition, also the  $\pi^- \pi^+$  invariant mass distribution shows some difference between events from  $\Phi \rightarrow \tau^- \tau^+$  and  $Z \rightarrow \tau^- \tau^+$  [32]. Rather than trying to discriminate against the irreducible background, an alternative strategy might be, for a light  $\Phi$ , to take into account the  $Z \rightarrow \tau^- \tau^+$  events both in the measurement and in the Monte Carlo modeling of the distributions (9) and (10). This requires a detailed study which is, however, beyond the scope of this paper.

### E. Higgs-sector $CP$ violation

Besides  $\varphi^*$ , a further important observable in this context is the angle  $\psi_{CP}^*$  defined in (10). It is the appropriate variable to check whether or not a spin-zero resonance  $\Phi$  has couplings to both scalar and pseudoscalar  $\tau$  lepton currents. A nontrivial  $\psi_{CP}^*$  distribution, respectively a nonzero asymmetry associated with this distribution would be evidence for  $CP$  violation in the ‘‘Higgs sector’’ (which is different from Kobayashi-Maskawa  $CP$  violation). Such a discovery would have enormous consequences, in particular for baryogenesis scenarios (see, e.g., the reviews [34, 35]).

We assume here that  $\Phi$  is an ideal mixture of a  $CP$ -even and  $CP$ -odd spin-zero state, with

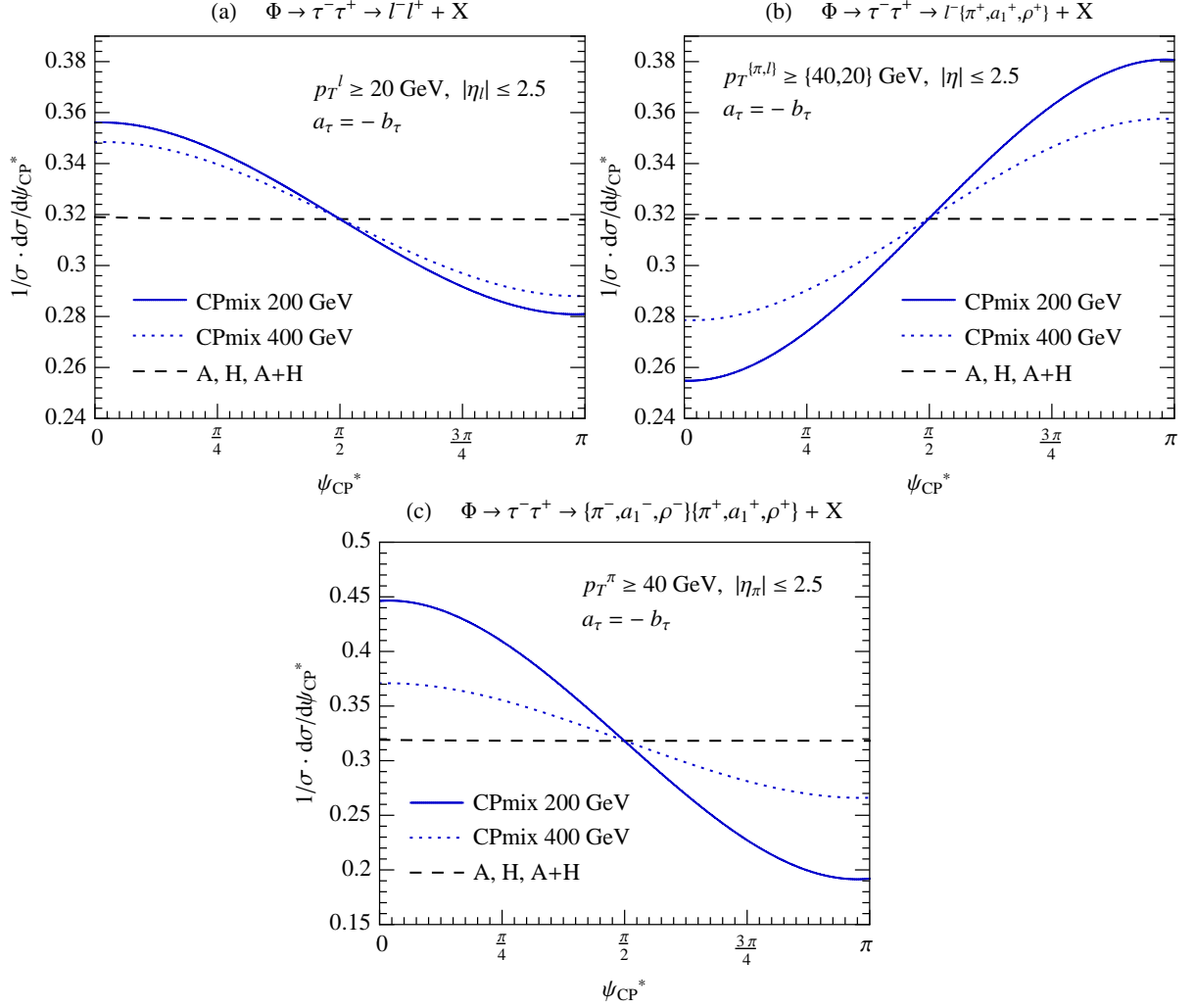


Figure 12: The  $\psi_{CP}^*$  distributions for (a) dilepton, (b) lepton-pion, and (c) two-pion final states. The different scenarios are explained in the text.

reduced Yukawa couplings  $a_\tau = -b_\tau$  to  $\tau$  leptons<sup>8</sup>. For definiteness, we take  $a_\tau = -b_\tau = 1$ . We call this the *CPmix* scenario for short and consider it for a Higgs-boson with mass  $m_\Phi = 200$  and 400 GeV. For comparison we consider also three scenarios where *CP* is conserved: i) a pure scalar *H*, ii) a pure pseudoscalar *A*, and iii) the case of a (nearly) mass-degenerate scalar *H* and pseudoscalar *A* with approximately the same production cross section and decay rate into  $\tau$  leptons.

The distribution of  $\psi_{CP}^*$  is displayed in Figs. 12(a) - (c) for dilepton, lepton-pion, and two-pion final states, respectively. The figures show that the variable  $\psi_{CP}^*$  efficiently distinguishes between *CP* conservation and violation – for the *CP*-conserving scenarios i) - iii) above, the distribution is flat. For a *CP*-mixed state, the slope of the  $\psi_{CP}^*$  distribution for lepton-pion

<sup>8</sup> Suffice it to mention that for the normalized  $\psi_{CP}^*$  distribution only the relative magnitude and phase of  $a_\tau$  and  $b_\tau$  matter, while the magnitudes of these couplings determine the decay rate of  $\Phi \rightarrow \tau\tau$ .

$m_\Phi$ [GeV]	dilepton	lepton-pion	two-pion
200	1540	514	116
400	2400	1390	726

Table IV: Event numbers needed to find evidence with 3 s.d. significance that  $\Phi$  is an ideal  $CP$  mixture.

final states is opposite in sign to the slope for dilepton and for two-pion final states, for reasons mentioned above. In analogy to (14) one may consider the asymmetry

$$A_{\psi_{CP}^*} = \frac{N(\psi_{CP}^* > \pi/2) - N(\psi_{CP}^* < \pi/2)}{N(\psi_{CP}^* > \pi/2) + N(\psi_{CP}^* < \pi/2)}. \quad (15)$$

With the values of  $A_{\psi_{CP}^*}$  obtained from the distributions Figs. 12(a) - (c) one gets the estimates of the event numbers, given in Table IV, that are needed to find evidence with 3 s.d. significance that  $\Phi$  is an ideal  $CP$  mixture.

One may enhance the discriminating power of the  $\psi_{CP}^*$  distribution by constructing an approximate Higgs-boson rest frame as outlined in Sec. III C and impose additional cuts on the energies of the charged-pions in this frame. In analogy to the above results for the  $\varphi^*$  distribution, we find that the improvement as compared to the results shown in Figs. 12(b), (c) is small for Higgs-boson masses below 200 GeV, whereas it becomes significant for heavy  $CP$  mixtures with  $m_\Phi \sim 400$  GeV.

#### IV. CONCLUSIONS

We have shown that the  $CP$  quantum numbers of a Higgs-boson  $\Phi$ , produced at the LHC, can be determined with the observables (9) and (10) in the  $\tau$ -decay mode  $\Phi \rightarrow \tau^+ \tau^-$ , using all major subsequent 1-prong  $\tau$  decays. The selection cuts that we applied in our analysis to the dilepton, lepton-pion, and two-pion final states significantly enhance the discriminating power of these observables for the “non direct charged-pion decay modes”. Therefore, practically all  $\tau$  decay modes can be used for pinning down the  $CP$  properties of  $\Phi$ , because the three-prong  $\tau$  decays can also be employed for this purpose [18]. Depending on the  $\Phi$ -production cross sections, i.e., on its mass and couplings, it should be feasible to collect the event numbers (estimated in Tables III and IV) that are required for statistically significant  $CP$  measurements after several years of high-luminosity runs at the LHC.

#### APPENDIX

In this appendix we collect, for the convenience of the reader, some results on  $\tau$  decays which are relevant for the calculations described above. (For a review, see [36].) The branching ratios of the 1-prong  $\tau$ -decay modes, given in Table V, are taken from [37].

decay mode	$\tau^\pm \rightarrow \pi^\pm$	$\tau^\pm \rightarrow \rho^\pm \rightarrow \pi^\pm \pi^0$	$\tau^\pm \rightarrow a_1^\pm \rightarrow \pi^\pm 2\pi^0$	$\tau^\pm \rightarrow e^\pm, \mu^\pm$
$BR_{PDG}$ [%]	10.91	25.51	9.3	35.2

Table V: Branching ratios for the major 1-prong  $\tau$ -decay modes [37].

Next we list the spectral functions  $n(E_a)$  and  $b(E_a)$  of the energy-angular distributions (8) of polarized  $\tau^\mp$  decays to  $a^\mp$ . The functions given below apply to both  $\tau^-$  and  $\tau^+$  – but notice the sign change in front of  $b(E_a)$  in (8). Furthermore, our convention for the distribution (8) is such that we differentiate with respect to the energy  $E_a$  of the charged prong. Therefore, the functions  $n(E_a)$  are dimensionful while the functions  $b(E_a)$  are dimensionless.

**The decay  $\tau^\mp \rightarrow \pi^\mp + \nu_\tau$**

In the 2-body decay  $\tau \rightarrow \pi + \nu_\tau$  the energy  $E_\pi$  in the  $\tau$  rest frame is fixed and the functions  $n_\pi(E_\pi)$  and  $b_\pi(E_\pi)$  are given by [38]:

$$n_\pi(E_\pi) = \delta\left(E_\pi - \frac{m_\tau^2 + m_\pi^2}{2m_\tau}\right), \quad b_\pi(E_\pi) = 1. \quad (16)$$

**The decay  $\tau^\mp \rightarrow \rho^\mp \rightarrow \pi^\mp \pi^0 \nu_\tau$**

The differential rate of the decay of polarized  $\tau$  leptons to a charged pion via a  $\rho$ -meson was calculated in [38]. With  $x = 4E_\pi/m_\tau$ , where  $E_\pi$  denotes the energy of the charged-pion in the  $\tau$  rest frame, the spectral functions are given by

$$n_\rho(E_\pi) = \frac{6}{m_\tau} \frac{(x-r-1)^2 + (1-r)(r-p)}{(1-r)^2(1+2r)(1-p/r)^{3/2}},$$

$$b_\rho(E_\pi) = \frac{x(x-r-1)^2 + x(3-r)(r-p) - 4(r-p)}{\sqrt{x^2 - 4p}((x-r-1)^2 + (1-r)(r-p))},$$

with  $p = 4m_\pi^2/m_\tau^2$  and  $r = m_\rho^2/m_\tau^2$ . These functions are plotted in Fig. 4(a). The kinematic range of  $E_\pi$  is

$$\frac{m_\tau}{4} \left(1 + r - (1-r)\sqrt{1 - \frac{p}{r}}\right) \leq E_\pi \leq \frac{m_\tau}{4} \left(1 + r + (1-r)\sqrt{1 - \frac{p}{r}}\right). \quad (17)$$

**The decay  $\tau^\mp \rightarrow a_1^\mp \rightarrow \pi^\mp 2\pi^0 \nu_\tau$**

The differential rate of the 1-prong decay of polarized  $\tau$  leptons to a charged-pion via a  $a_1$ -meson was calculated in [39]. The corresponding functions  $n_{a_1}(E_\pi)$  and  $b_{a_1}(E_\pi)$  are complicated and were fitted to the numerical results shown in Fig. 6-4 of Ref. [39]. With

$$x = \frac{2m_\tau(E_\pi - m_\pi)}{m_\tau^2 - 3m_\pi^2 - 2m_\tau m_\pi} \quad (18)$$



where  $E_\pi$  is the energy of the charged-pion in the  $\tau$  rest frame, we obtain

$$n_{a_1}(E_\pi) = \frac{2m_\tau}{m_\tau^2 - 3m_\pi^2 - 2m_\tau m_\pi} \left( 0.0112624 - 2.15495x + 165.368x^2 - 997.586x^3 + 2818.75x^4 - 4527.77x^5 + 4250.43x^6 - 2182.33x^7 + 475.283x^8 \right), \quad (19)$$

$$b_{a_1}(E_\pi) = -5.28726\sqrt{x} + 9.38612x - 1.26356x^2 - 18.9094x^3 + 36.0517x^4 - 19.4113x^5. \quad (20)$$

The plots of  $n_{a_1}(E_\pi)$  and  $b_{a_1}(E_\pi)$  are shown in Fig. 4(b). The kinematical range of the charged-pion energy in the  $\tau$  rest frame is

$$m_\pi \leq E_\pi \leq \frac{m_\tau^2 - 3m_\pi^2}{2m_\tau}. \quad (21)$$

### The decay $\tau^\mp \rightarrow l^\mp \nu_l \nu_\tau$

For the leptonic decays  $\tau^\pm \rightarrow l^\pm \nu_l \nu_\tau$  the mass of the final state lepton,  $e$  or  $\mu$ , can be neglected. Using  $x = 2E_l/m_\tau$ , where  $E_l$  is defined in the  $\tau$  rest frame, one has [38]

$$n_l(E_l) = \frac{4}{m_\tau} x^2 (3 - 2x), \quad b_l(E_l) = \frac{1 - 2x}{3 - 2x} \quad (22)$$

with  $0 \leq E_l \leq m_\tau/2$ .

### Acknowledgments

The work of S. B. is supported by the Initiative and Networking Fund of the Helmholtz Association, Contract No. HA-101 (“Physics at the Terascale”) and by the Research Center “Elementary Forces and Mathematical Foundations” of the Johannes-Gutenberg-Universität Mainz. The work of W. B. is supported by BMBF.

- 
- [1] S. Berge and W. Bernreuther, Phys. Lett. **B671**, 470 (2009). [arXiv:0812.1910 [hep-ph]].
  - [2] A. Djouadi, Phys. Rept. **457**, 1 (2008); [arXiv:hep-ph/0503172].
  - [3] A. Djouadi, Phys. Rept. **459**, 1 (2008); [arXiv:hep-ph/0503173].
  - [4] M. Gomez-Bock, M. Mondragon, M. Mühlleitner, M. Spira and P. M. Zerwas, “Concepts of Electroweak Symmetry Breaking and Higgs Physics,” [arXiv:0712.2419 [hep-ph]].
  - [5] C. Grojean, Phys. Usp. **50**, 1 (2007).
  - [6] D. E. Morrissey, T. Plehn and T. M. P. Tait, “Physics searches at the LHC,” [arXiv:0912.3259 [hep-ph]].

- [7] J. R. Dell’Aquila and C. A. Nelson, Phys. Rev. D **33**, 80 (1986).
- [8] J. R. Dell’Aquila and C. A. Nelson, Nucl. Phys. B **320**, 86 (1989).
- [9] W. Bernreuther and A. Brandenburg, Phys. Lett. B **314**, 104 (1993); Phys. Rev. D **49**, 4481 (1994).
- [10] D. Chang, W. Y. Keung and I. Phillips, Phys. Rev. D **48**, 3225 (1993).
- [11] A. Soni, R. M. Xu, Phys. Rev. **D48**, 5259 (1993). [hep-ph/9301225].
- [12] M. Krämer, J. H. Kühn, M. L. Stong and P. M. Zerwas, Z. Phys. C **64**, 21 (1994).
- [13] B. Grzadkowski and J. F. Gunion, Phys. Lett. B **350**, 218 (1995).
- [14] W. Bernreuther, A. Brandenburg and M. Flesch, Phys. Rev. D **56**, 90 (1997). [hep-ph/9701347].
- [15] T. Plehn, D. L. Rainwater and D. Zeppenfeld, Phys. Rev. Lett. **88**, 051801 (2002).
- [16] C. P. Buszello *et al.*, Eur. Phys. J. C **32**, 209 (2004).
- [17] G. Klamke and D. Zeppenfeld, JHEP **0704**, 052 (2007). [hep-ph/0703202 [HEP-PH]].
- [18] S. Berge, W. Bernreuther and J. Ziethe, Phys. Rev. Lett. **100**, 171605 (2008). [arXiv:0801.2297 [hep-ph]].
- [19] A. De Rujula, J. Lykken, M. Pierini, C. Rogan and M. Spiropulu, Phys. Rev. **D82**, 013003 (2010). [arXiv:1001.5300 [hep-ph]].
- [20] E. Accomando *et al.*, “Workshop on CP Studies and Nonstandard Higgs Physics,” [hep-ph/0608079].
- [21] J. Baglio, A. Djouadi, JHEP **1103**, 055 (2011). [arXiv:1012.0530 [hep-ph]].
- [22] J. Baglio, A. Djouadi, [arXiv:1103.6247 [hep-ph]].
- [23] S. Chatrchyan *et al.* [CMS Collaboration], Phys. Rev. Lett. **106**, 231801 (2011). [arXiv:1104.1619 [hep-ex]]; CMS Collaboration, CMS PAS HIG-11-009.
- [24] G. Aad *et al.* [ATLAS Collaboration], Phys. Lett. B **705**, 174 (2011).
- [25] R. Harlander, J. Phys. G **G35**, 033001 (2008).
- [26] S. Dittmaier *et al.* [LHC Higgs Cross Section Working Group Collaboration], “Handbook of LHC Higgs Cross Sections: 1. Inclusive Observables,” [arXiv:1101.0593 [hep-ph]].
- [27] R. K. Ellis, I. Hinchliffe, M. Soldate and J. J. van der Bij, Nucl. Phys. **B297**, 221 (1988).
- [28] A. Elagin, P. Murat, A. Pranko and A. Safonov, Nucl. Instrum. Methods Phys. Res., Sect. A **654**, 481 (2011). [arXiv:1012.4686 [hep-ex]].
- [29] L. Perchalla, Ph.D. thesis, “Kinematic Tau Reconstruction and Search For The Higgs Boson in Hadronic Tau Pair Decays with the CMS Experiment”, RWTH Aachen (2011).
- [30] W. Bernreuther, O. Nachtmann, Phys. Rev. Lett. **63**, 2787 (1989).
- [31] W. Bernreuther, O. Nachtmann, P. Overmann, Phys. Rev. **D48**, 78 (1993).
- [32] T. Pierzchala, E. Richter-Was, Z. Was, M. Worek, Acta Phys. Polon. **B32**, 1277 (2001). [hep-ph/0101311].
- [33] P. L. Rosendahl, T. Burgess, B. Stugu, [arXiv:1105.6003 [hep-ex]].
- [34] A. G. Cohen, D. B. Kaplan and A. E. Nelson, Ann. Rev. Nucl. Part. Sci. **43**, 27 (1993).
- [35] W. Bernreuther, Lect. Notes Phys. **591**, 237 (2002). [hep-ph/0205279].

- [36] A. Stahl, Springer Tracts Mod. Phys. **160**, 1 (2000).
- [37] K. Nakamura *et al.* [Particle Data Group Collaboration], J. Phys. G **G37**, 075021 (2010).
- [38] Y. -S. Tsai, Phys. Rev. **D4**, 2821 (1971); Erratum-ibid. **D13**, 771 (1976).
- [39] P. Overmann, Ph.D. thesis, Universität Heidelberg, 1992, preprint HD-THEP-92-38.